

Inelastic neutron scattering study of the intra-lanthanide alloys $\text{Er}_x\text{Pr}_{1-x}$ ($x=0.6,0.8$)Th. Strässle,^{1,*} S. Janssen,¹ F. Juranyi,¹ A. Furrer,¹ O. Moze,² A. O. Pecharsky,³ V. K. Pecharsky,³ and K. A. Gschneidner, Jr.³¹Laboratory for Neutron Scattering, ETH Zürich & PSI, 5232 Villigen PSI, Switzerland²INFN, Dipartimento di Fisica, Università di Modena e Reggio Emilia, Modena 41100, Italy³Ames Laboratory and Department of Materials Science and Engineering, Iowa State University, Ames, Iowa 50011-3020, USA

(Received 6 January 2003; revised manuscript received 3 June 2003; published 7 October 2003)

Neutron spectroscopy has been applied in order to elucidate the magnetothermal properties of the lanthanide alloys $\text{Er}_x\text{Pr}_{1-x}$ ($x=0.6,0.8$). The observed crystal-field splittings are in accordance with the arithmetically weighted crystal fields of the two pure metals. A mean-field approach is presented, which couples the two effective internal fields originating from the Er and Pr ions. The model is successful in explaining many of the observed magnetic properties, including the ferrimagnetic arrangement of the Er and Pr moments, the values of the respective moments, the magnetocaloric effect for $x=0.7$ and the large increase of the magnetic entropy at low temperatures due to the addition of Pr. A large single-ion anisotropy is derived and it is predicted that an enhanced magnetocaloric effect should be observed in single-crystal samples for $x\sim 0.7$ with the external magnetic field applied along the c axis. Additional magnetization measurements under pressure up to 0.72 GPa have shown no evidence for a pronounced sensitivity of the magnetic ordering temperature upon pressure in $\text{Er}_{0.6}\text{Pr}_{0.4}$.

DOI: 10.1103/PhysRevB.68.134411

PACS number(s): 75.30.Sg, 75.10.Dg, 25.40.Fq, 74.62.Fj

I. INTRODUCTION

Both passive and active magnetic refrigeration have gained increasing interest in recent years. Most of the materials considered for cooling applications are based on lanthanide compounds because of their large magnetic moments. In passive magnetic refrigeration no magnetic field is applied, but the high heat capacity due to magnetic ordering is essential in the use of lanthanide materials as regenerator materials to attain temperatures below 10–15 K.^{1,2}

In active magnetic refrigeration an applied magnetic field is utilized to produce a temperature change, but in this case it is the magnetocaloric effect (MCE) associated with the coupling of a spin system with the magnetic field that plays an important role.^{3,4} In addition in most of the cases the lanthanide material is also used as a regenerator in the refrigeration process, where a large heat capacity is important. However, a large heat capacity is a double edge sword—useful in the regeneration process, but it leads to internal heat (entropy) losses as the magnetic refrigerant is cycled from high temperature to low temperature, and reverse.

In the intra-lanthanide alloys $\text{Er}_x\text{Pr}_{1-x}$ the addition of Pr has been found to lead to a substantial increase of the heat capacity at low temperatures, which makes them promising candidates as passive magnetic refrigerants at temperatures between 10 K and 80 K. However, as pointed out by Wu *et al.*⁵ the $\text{Er}_x\text{Pr}_{1-x}$ alloys for $x=0.7$ exhibits a sharp heat-capacity peak at ~ 35 K and a narrow caretlike MCE peak at this temperature. The MCE is reasonably large and thus this alloy is also a promising active magnetic refrigerant at ~ 35 K in addition to being an excellent passive magnetic regenerator material for cooling down to ~ 10 K.

$\text{Er}_x\text{Pr}_{1-x}$ has been studied by measurements of the heat capacity, dc magnetization, and ac magnetic susceptibility at varying magnetic fields in order to investigate its magnetic properties and to determine indirectly the MCE.⁵ Pure Er

exhibits an antiferromagnetic phase below $T_N\sim 85$ K and then two intermediate magnetic transitions (53 K and 26 K), followed by a first-order transition at $T_C=19$ K. Pr additions were found to decrease the Néel temperature while increasing the Curie temperature eventually leading to the merge of the two ordering temperatures for $x\sim 0.6$ in $\text{Er}_x\text{Pr}_{1-x}$. Recent neutron diffraction experiments^{6,7} on the magnetic structure of $\text{Er}_x\text{Pr}_{1-x}$ have determined for the alloy $\text{Er}_{0.6}\text{Pr}_{0.4}$ a ferrimagnetic alignment with opposed Er and Pr moments along the c axis for all temperatures up to the Curie point of 35 K. For the alloy $\text{Er}_{0.8}\text{Pr}_{0.2}$, the site moments were found to be aligned ferromagnetically along the c axis for $T<30$ K, while for $T>35$ K a c axis sinusoidal modulation was observed. Between 30 and 35 K, the moments were found to have both ferromagnetic c axis and sinusoidally modulated components.

The above studies have begun to elucidate the magnetic phase diagram of $\text{Er}_x\text{Pr}_{1-x}$ both on the macroscopic and microscopic levels for $x\leq 0.8$. Nonetheless for a modeling of the heat capacity and corresponding entropy, the crystalline electric field (CF) must be considered, as it constitutes the carrier of the magnetic entropy in a pure lanthanide material. Hence we have applied inelastic neutron scattering on $\text{Er}_{0.6}\text{Pr}_{0.4}$ and $\text{Er}_{0.8}\text{Pr}_{0.2}$ to establish the CF with the aim of reconstructing the magnetic as well as magnetothermal properties of $\text{Er}_x\text{Pr}_{1-x}$ for $x\leq 0.7$ on the basis of microscopic parameters. The presented scheme may well be applied to other MCE compounds for which currently no microscopic description of the MCE is available. Thus, it may help in finding optimized MCE materials.

II. EXPERIMENTAL PROCEDURE

Polycrystalline samples of $\text{Er}_{0.6}\text{Pr}_{0.4}$ and $\text{Er}_{0.8}\text{Pr}_{0.2}$ were prepared following an arc-melting, heat treatment procedure as described elsewhere.^{5,6} The inelastic neutron-scattering

measurements were carried out on the time-of-flight spectrometer FOCUS at the neutron spallation source SINQ in Switzerland with an incoming neutron energy of $E_i = 12.0$ meV and time focusing at 4 meV energy loss. The samples were placed in Al cans of 10 mm diameter. They were cooled in a closed-cycle refrigerator ($x=0.6$) and a He cryostat ($x=0.8$). The measurements of the ac magnetic susceptibility of $\text{Er}_{0.6}\text{Pr}_{0.4}$ were carried out on a Quantum Design physical properties measurement system. A clamp cell made of nonmagnetic Cu/Be alloy was used allowing for pressures up to 1 GPa. Within the cell the sample was placed in a thin capsule made of lead and filled with Fluorinert FC-77. The superconducting transition temperature of lead was used to measure the pressure.⁸

III. THEORETICAL BACKGROUND

Pure Er crystallizes in the normal hcp structure, whereas pure Pr crystallizes in the double hcp structure (both belong to space group $P6_3/mmc$). The disordered alloy $\text{Er}_x\text{Pr}_{1-x}$ ($x \geq 0.6$) crystallizes in the hcp structure like Er.⁶ The hexagonal point symmetry around the lanthanide ion gives rise to a CF described in Stevens notation by⁹

$$\hat{\mathcal{H}}^{\text{CF}} = B_2^0 \hat{O}_2^0 + B_4^0 \hat{O}_4^0 + B_6^0 \hat{O}_6^0 + B_6^6 \hat{O}_6^6 \quad (1)$$

with B_n^m and \hat{O}_n^m the Stevens CF parameters and operators, respectively. The $(2J_{\text{Er}} + 1 = 16)$ -fold-degenerate ground-state J multiplet of Er is thus split into eight Kramers doublets, whereas the $(2J_{\text{Pr}} + 1 = 9)$ -fold-degenerate ground-state J multiplet of Pr is split into three singlet and three doublet states. In the magnetically ordered state the CF levels become further split by the effective molecular fields from the Er and Pr ions, respectively (Zeeman effect). In a simple one-lattice mean-field approach the corresponding internal fields are¹⁰

$$g_{\text{Er}} \mu_B \mathbf{H}_{\text{Er}} = -\lambda_{\text{Er-Er}} x \langle \hat{\mathbf{J}}_{\text{Er}} \rangle - \lambda_{\text{Er-Pr}} (1-x) \langle \hat{\mathbf{J}}_{\text{Pr}} \rangle, \quad (2)$$

$$g_{\text{Pr}} \mu_B \mathbf{H}_{\text{Pr}} = -\lambda_{\text{Pr-Pr}} (1-x) \langle \hat{\mathbf{J}}_{\text{Pr}} \rangle - \lambda_{\text{Er-Pr}} x \langle \hat{\mathbf{J}}_{\text{Er}} \rangle, \quad (3)$$

with $\lambda_{\text{Er-Er}}$, $\lambda_{\text{Pr-Pr}}$, and $\lambda_{\text{Er-Pr}}$ the exchange parameters between ions of the same and different kind, respectively, $\hat{\mathbf{J}}_{\text{Er}}$ and $\hat{\mathbf{J}}_{\text{Pr}}$ are the total angular momentum of Er and Pr, respectively and x the Er concentration. The three exchange parameters are governed by the de Gennes factor

$$\lambda_{r-s} \propto (g_r - 1)(g_s - 1) j_{sf}^2, \quad r, s \in \{\text{Er}, \text{Pr}\}. \quad (4)$$

With constant sf -coupling j_{sf} and $g_{\text{Er}} = 6/5$ and $g_{\text{Pr}} = 4/5$ one finds $\lambda_{\text{Er-Er}} = \lambda_{\text{Pr-Pr}} = -\lambda_{\text{Er-Pr}} \equiv \lambda$. Thus the magnetic moments of Er and Pr are expected to align ferrimagnetically in accordance with the neutron-diffraction results.⁶ The effective single-ion Hamiltonians for the Er and Pr ions are given by

$$\hat{\mathcal{H}}_{\text{Er}} = \hat{\mathcal{H}}_{\text{Er}}^{\text{CF}} + g_{\text{Er}} \mu_B (\mathbf{H}_{\text{Er}} + \mathbf{H}_{\text{ext}}) \hat{\mathbf{J}}_{\text{Er}}, \quad (5)$$

$$\hat{\mathcal{H}}_{\text{Pr}} = \hat{\mathcal{H}}_{\text{Pr}}^{\text{CF}} + g_{\text{Pr}} \mu_B (\mathbf{H}_{\text{Pr}} + \mathbf{H}_{\text{ext}}) \hat{\mathbf{J}}_{\text{Pr}}, \quad (6)$$

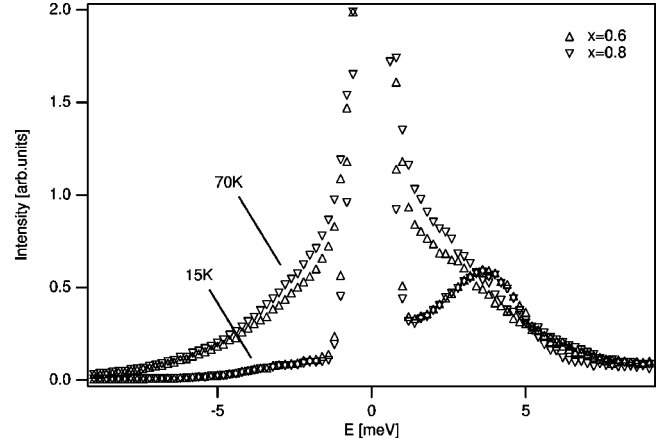


FIG. 1. Observed inelastic neutron spectra for $\text{Er}_{0.6}\text{Pr}_{0.4}$ and $\text{Er}_{0.8}\text{Pr}_{0.2}$ ($T=15$, and 70 K, data scaled to match approximate overall intensities).

where we have also included the effect of an external magnetic field \mathbf{H}_{ext} . The above equations fully define the single-ion eigenstates Γ_n , and eigenvalues E_n , which in turn determine the magnetic properties of interest, such as magnetic moment per Er (Pr) ion

$$\langle \mu^\alpha \rangle |r\rangle = g_r \mu_B \sum_n p_n \langle \Gamma_n | J^\alpha | \Gamma_n \rangle |r\rangle,$$

$$\alpha = x, y, z, \quad r \in \{\text{Er}, \text{Pr}\}, \quad (7)$$

with $p_n = e^{-E_n/k_B T} / Z$ the thermal population factors at temperature T .⁹ Similarly, the magnetic entropy per ion is given by

$$S_m |r\rangle = -k_B \sum_n p_n \ln p_n |r\rangle, \quad r \in \{\text{Er}, \text{Pr}\}. \quad (8)$$

It should be noted that this expression remains valid also in the magnetically ordered state.¹¹ The magnetic entropy per mole $\text{Er}_x\text{Pr}_{1-x}$ is thus

$$S_m = N_A [x S_m |_{\text{Er}} + (1-x) S_m |_{\text{Pr}}], \quad (9)$$

where N_A is Avogadro's constant.

IV. RESULTS AND DATA ANALYSIS

Figure 1 shows the observed inelastic neutron spectra for $\text{Er}_{0.6}\text{Pr}_{0.4}$ and $\text{Er}_{0.8}\text{Pr}_{0.2}$ taken above and below the magnetic ordering temperature T_0 . The two compositions show similar characteristics. The CF transitions are not resolved but rather give rise to wide wings around the elastic line in the paramagnetic state and a broad bump in the magnetically ordered state. Because of the lack of structure in the spectra, care must be exercised in parametrizing the CF. Further information can be gained by studying the temperature dependence of the two alloys. Figures 2 and 3 illustrate the temperature dependence of $\text{Er}_{0.6}\text{Pr}_{0.4}$ ($T_C = 35$ K) and $\text{Er}_{0.8}\text{Pr}_{0.2}$ ($T_N = 49$ K, $T_C = 33$ K). The CFs of the pure lanthanide metals

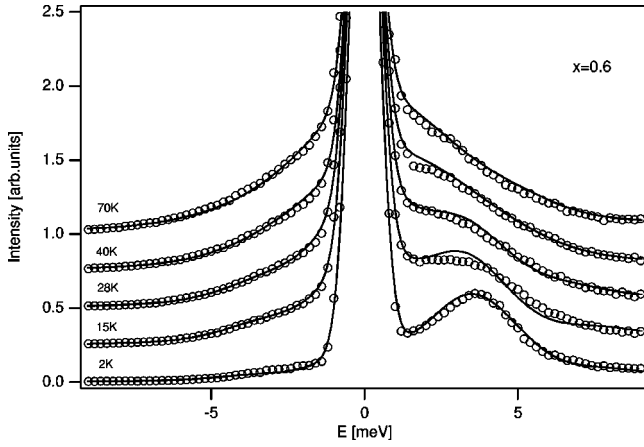


FIG. 2. Observed inelastic neutron spectra for $\text{Er}_{0.6}\text{Pr}_{0.4}$ and fit at different temperatures (the parameters for the fit are listed in Table I).

Er and Pr (in hcp structure) have been determined earlier by Touborg *et al.*^{12,13} Starting from these values by a mere arithmetic weighting of the two CFs by the Er concentration x , the calculated overall splitting of the CF turns out to be about 20% too large. This mismatch to the experimentally observed overall splitting may be expected, since the above CF parameters for the pure metals have been derived from dilution of Er (Pr) into a matrix of nonmagnetic La, Lu, or Y giving rise to altered lattice parameters.

Since the two sixth-order CF parameters are responsible for the size of the overall CF splitting, we have fitted B_6^0 independently for Er and Pr. Furthermore, we have released the constraint $B_6^{\text{Er}}/B_6^{\text{Pr}} = 77/8$, which has been applied in the earlier works by Touborg *et al.*^{12,13} and which strictly is valid only for a simple point-charge model with the ideal lattice parameter ratio $c/a = 1.633$ ($\text{Er}_{0.6}\text{Pr}_{0.4}$, $c/a = 1.582$, and $\text{Er}_{0.8}\text{Pr}_{0.2}$, $c/a = 1.576$).⁶ However, in view of the random allocation of Er and Pr one must consider equal local geometry for the Er and Pr ions, and therefore, must assume an equal ratio $B_6^{\text{Er}}/B_6^{\text{Pr}}$ in the two single-ion Hamiltonians [Eqs. (5) and (6)]. The second- and fourth-order CF parameters

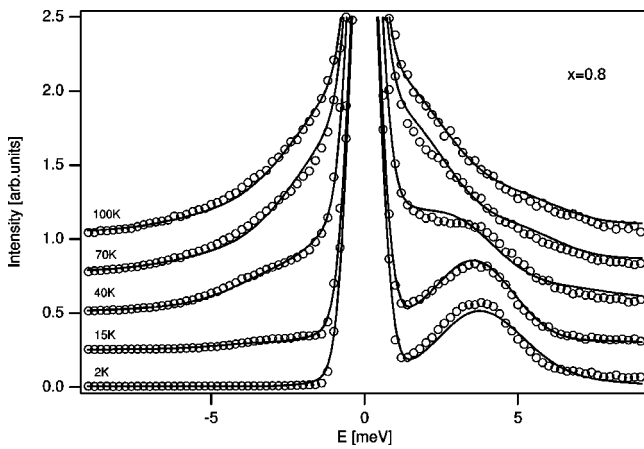


FIG. 3. Observed inelastic neutron spectra for $\text{Er}_{0.8}\text{Pr}_{0.2}$ and fit at different temperatures (the parameters for the fit are listed in Table I).

TABLE I. Best-fit parameters for the CF and the molecular field in $\text{Er}_{0.6}\text{Pr}_{0.4}$ and $\text{Er}_{0.8}\text{Pr}_{0.2}$, interpolated values for $\text{Er}_{0.7}\text{Pr}_{0.3}$ [all values in meV, fixed values $B_2^0(\text{Er}) = -0.201 \times 10^{-1}$, $B_4^0(\text{Er}) = 0.379 \times 10^{-4}$, $B_2^0(\text{Pr}) = 0.127$, $B_4^0(\text{Pr}) = -0.272 \times 10^{-3}$ meV from Refs. 12,13].

x	$B_6^0 _{\text{Er}} \times 10^5$	$B_6^0 _{\text{Pr}} \times 10^4$	$B_6^0 _{\text{Pr}} \times 10^4$	$B_6^0 _{\text{Pr}} \times 10^3$	λ
0.6	0.178(23)	0.237(42)	0.96(20)	1.28(23)	0.204(14)
0.8	0.179(29)	0.263(47)	0.64(47)	0.94(17)	0.194(16)
0.7	0.178	0.249	0.864	1.085	0.199

have been fixed to the values found by Touborg. In addition to $B_6^0|_{\text{Er}}$, $B_6^0|_{\text{Pr}}$, and $B_6^{\text{Er}}/B_6^{\text{Pr}}$, we have fitted (i) the intensity of the elastic line, (ii) a constant intrinsic broadening of the CF transitions, (iii) the molecular-field parameter λ , and (iv) the intensity of the quasielastic scattering in the magnetically ordered state. The instrumental resolution was kept fixed to the calculated values. The spectra were fitted pairwise for $T < T_0$ and $T > T_0$ yielding two parameter sets for $\text{Er}_{0.6}\text{Pr}_{0.4}$ and $\text{Er}_{0.8}\text{Pr}_{0.2}$ to enable us to describe all measured temperatures. The respective parameters B_n^m and λ are listed in Table I. The fits are shown as solid lines in Figs. 2 and 3. The parametrization of the CF is able to describe the observed temperature dependence and the Zeeman split state. The two sets for $\text{Er}_{0.6}\text{Pr}_{0.4}$ and $\text{Er}_{0.8}\text{Pr}_{0.2}$ are consistent with one another. Within the error, the two mean-field parameters for $x = 0.6$ and $x = 0.8$ are equal and of reasonable size (see the following section). An intrinsic broadening of the CF transitions as large as 2.5 meV and 2.75 meV for $T > T_0$ and $T < T_0$, respectively, is derived from the fit, which explains the unshaped nature of the spectra. Several factors add to the observed intrinsic broadening in $\text{Er}_x\text{Pr}_{1-x}$, including (i) magnetic dispersion, which is expected to be large in view of the relatively high ordering temperatures, (ii) differences in the metallic radii of Er and Pr giving rise to a local distorted lattice, and (iii) the large difference in the magnetic moments of Er and Pr (see below) resulting in a locally inhomogeneous magnetic field.

V. DISCUSSION

A. Magnetic properties

Considering the lack of structure in the spectra, the derived CF parameters and molecular constants must be compared with the thermodynamic and magnetic properties of the alloy. We reconstruct these properties for the case of $\text{Er}_{0.7}\text{Pr}_{0.3}$ for which macroscopic measurements have been carried out and which shows a narrow region of the magnetically sine modulated structure (Refs. 5,6: $T_N \sim 34$ K, $T_C \sim 38$ K). The error weighted interpolated values of the CF parameters for $x = 0.7$ are listed in Table I. The components of the magnetic moments of Er and Pr can be readily calculated from Eq. (7). They are depicted in Fig. 4 for a zero magnetic field and an applied magnetic field $H_{\text{ext}} = 50$ kOe along the c axis. Let us first discuss the case $H_{\text{ext}} = 0$. Note that the ordering temperature as derived from the fitted mean-field parameter (Table I) is found to be somewhat

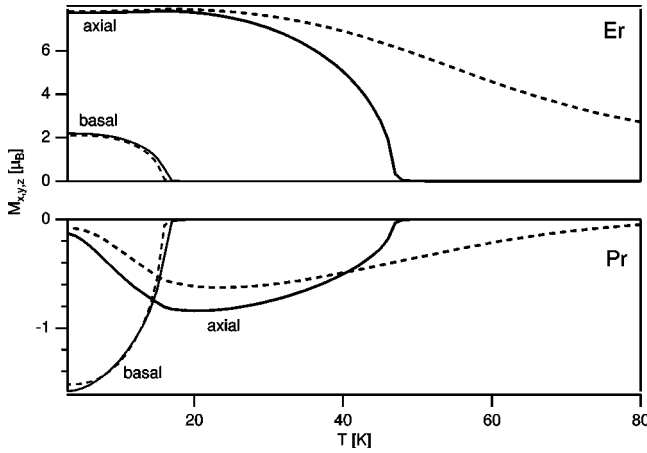


FIG. 4. The calculated magnetic moments of the Er ion and the Pr ion in $\text{Er}_{0.7}\text{Pr}_{0.3}$ without an external magnetic field (solid line) and in an applied field along the c axis of $H_{ext}=50$ kOe (dashed line). The calculations used the parameters given in Table I.

larger ($T_0 \sim 46$ K) than the experimentally determined value, a deviation which is often observed when using such a simple mean-field approach. Above around $T=18$ K the magnetic moments of Er and Pr align ferrimagnetically along the c axis with maximum values $\mu^z|_{\text{Er}}=7.83\mu_B$ and $\mu^z|_{\text{Pr}}=-0.83\mu_B$ per Er and Pr ion, respectively. The ferrimagnetic alignment is a consequence of Eq. (4) and is in accordance with the neutron-diffraction measurements on $\text{Er}_{0.6}\text{Pr}_{0.4}$ and $\text{Er}_{0.8}\text{Pr}_{0.2}$.⁶ As shown in Table II, the absolute values for the two moments are in good agreement with the effective magnetic moments μ_{eff} of $\text{Er}_x\text{Pr}_{1-x}$ derived from macroscopic measurements (i.e., by extrapolation of M_{DC} vs $1/H$ to $H \rightarrow 0$). With a ferrimagnetic alignment and a linear relationship upon the Er concentration x , one expects the effective magnetic moment to scale by

$$\mu_{\text{eff}} = x\mu_{\text{Er}} - (1-x)\mu_{\text{Pr}}. \quad (10)$$

Fitting the observed effective moments μ_{eff} obtained for the different alloys, x , to Eq. (10) (the first row of Table II), yields for the single-ion effective magnetic moments: $\mu_{\text{Er}}=8.0(1)\mu_B$ and $\mu_{\text{Pr}}=1.1(5)\mu_B$ (in the ferrimagnetically ordered state), which are in excellent agreement with the values reconstructed from the CF. The two single-ion magnetic moments are thus found to be considerably reduced by the CF as compared to their free ion values (gJ) of $9.0\mu_B$ for Er and $3.2\mu_B$ for Pr. The values for $x=0.6$ given in Table II may further be compared to recent neutron-diffraction measurements on $\text{Er}_{0.6}\text{Pr}_{0.4}$,⁷ which yield at 10 K a larger moment of $5.5(3)\mu_B$ aligned along the c axis. The moments of $\text{Er}_{0.8}\text{Pr}_{0.2}$ as observed by neutron-diffraction measurements⁷ in the ferromagnetic [$\mu_{\text{eff}}=7.2(3)\mu_B$ at $T=6$ K] and in the sinusoidally modulated phase [$\mu_{\text{eff}}=5.4(3)\mu_B$ at $T=35.6$ K] though may not be compared directly with Table II as our mean-field model supposes implicitly a ferrimagnetic alignment of the moments.

In the above mean-field calculations the Er and Pr ions develop magnetic moments with basal plane components for

TABLE II. Values of the effective magnetic moment μ_{eff} in $\text{Er}_x\text{Pr}_{1-x}$ observed by macroscopic measurements of the saturated magnetization [$T=4$ K and by fits to Eq. (10) $T \rightarrow 0$]. The fits give single-ion moments of $\mu_{\text{Er}}=8.0(1)$ and $\mu_{\text{Pr}}=1.1(5)$, which are in good agreement with values reconstructed from the CF: $\mu_{\text{Er}}=7.83$ and $\mu_{\text{Pr}}=0.83$ (all values in μ_B).

x	1.0	0.9	0.8	0.75	0.7	0.6
μ_{eff} (obs.)	7.87(9)	7.21(2)	6.31(3)	5.43(5)	5.21(8)	4.43(6)
μ_{eff} (fit)	7.95	7.05	6.15	5.70	5.25	4.35

$T < 17$ K (Fig. 4). The neutron-diffraction measurements^{6,7} on $\text{Er}_{0.6}\text{Pr}_{0.4}$ and $\text{Er}_{0.8}\text{Pr}_{0.2}$, however, did not show any evidence for a basal component of the magnetic moments of Er and Pr. The two basal contributions from Er and Pr may partially compensate each other resulting in a quite small total basal plane moment with respect to the large moment of Er along the c axis (note that the neutron-scattering intensities scale as the square of the magnetic moment). On the other hand, one may also reach the limits of the above simple mean-field ansatz, which though couples the two types of lanthanide ions but treats them in separate simple one-lattice models and which thus simplifies the true magnetic structure of the system. The tendency of Pr to develop a basal moment component becomes however understandable from its CF nature. Pure Pr has a nonmagnetic singlet ground state, and when subjected to an external magnetic field along the c axis, no magnetic moment may be induced up to a level crossing of the singlet with the first-excited (magnetic) doublet at a critical field of $H_c \approx 320$ kOe. Yet, if the external field is applied parallel to the basal plane, magnetic moments are readily induced by mixing of the two states.¹⁴

Finally, in the case of an applied magnetic field, we find that both lanthanide ions exhibit an induced magnetic moment already well above T_0 and when $T < T_0$ the value of the moments also change for $H_{ext} > 0$ (Fig. 4). This field dependence is the origin of the MCE discussed in the following section.

B. Magnetothermal and magnetoelastic properties

The above parametrization of the CF now allows us to derive the magnetothermal properties of the system. The magnetic entropy S_m may be readily calculated by use of Eq. (9) at $H_{ext}=0$ and $H_{ext}>0$. The total and partial magnetic entropies of $\text{Er}_{0.7}\text{Pr}_{0.3}$ are shown in Fig. 5 for $H_{ext}=0$ and $H_{ext}=50$ kOe along the c axis. Obviously, in Er the external magnetic field reduces S_m and broadens the kink in $S_m(T)$, which for $H_{ext}=0$ coincides with the magnetic ordering temperature of the system. On the other hand, the application of an external magnetic field has a minor influence on the magnetic entropy of Pr. As can be seen in Fig. 5, Pr contributes the most part of the magnetic entropy below $T \sim 10$ K. Hence Pr may be considered as an almost field-independent carrier of magnetic entropy, which increases the heat capacity of Er significantly at low temperatures.⁵ It is this feature which explains, on a microscopic level, the properties of $\text{Er}_x\text{Pr}_{1-x}$ ($x \sim 0.7$) being an excellent passive magnetic regenerator at ~ 10 K.

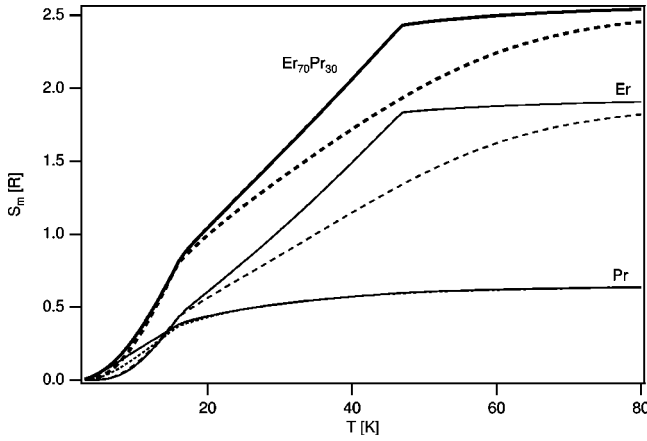


FIG. 5. The calculated magnetic entropy [Eq. (9)] originating from Er and Pr in $\text{Er}_{0.7}\text{Pr}_{0.3}$: the solid lines are for $H_{ext}=0$ and the dashed lines are for $H_{ext}=50$ kOe (using the parameters given in Table I).

On the basis of the calculated magnetic entropies $S_m(T, H_{ext}=0)$ and $S_m(T, H_{ext}>0)$, one may directly calculate the MCE $\Delta S = \Delta S_m = S_m^{H=0}(T) - S_m^{H>0}(T)$ (note that the lanthanide ions are the only carriers of the field-dependent entropy, hence $\Delta S = \Delta S_m$). The resulting MCE is shown in Fig. 6 in comparison with the values derived from heat-capacity and magnetization measurements on polycrystalline bulk samples.⁵ As a result of the higher ordering temperature obtained by the mean-field calculation (see the preceding section), the MCE is plotted against normalized temperature $(T-T_0)/T_0$. Due to the pronounced anisotropy of the system, the calculated MCE values are found to be distinctly larger than those measured on a polycrystalline sample. Vice versa the MCE of a single-crystal alloy is predicted to exhibit a pronounced dependence on the field direction. Note

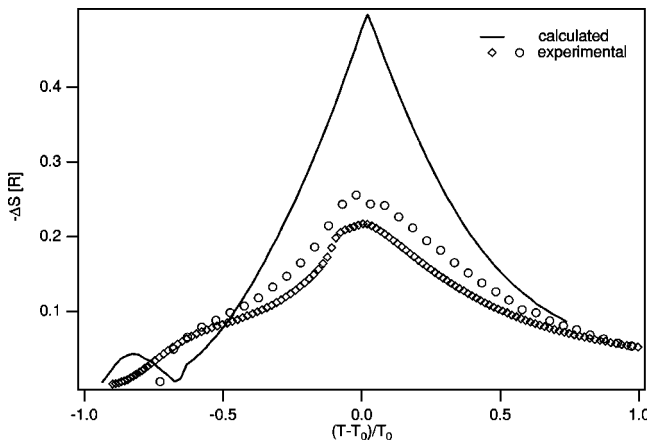


FIG. 6. The calculated MCE ΔS vs the reduced temperature for $\text{Er}_{0.7}\text{Pr}_{0.3}$ and $\Delta H_{ext} = 50$ kOe applied along the c axis (solid line). The MCE values obtained from measurements of the specific heat (diamonds) and the magnetization (circles) on a polycrystalline⁵ sample are also shown. $T_0 = T_C = 46$ and 39 K for the calculations and for the measurements, respectively.

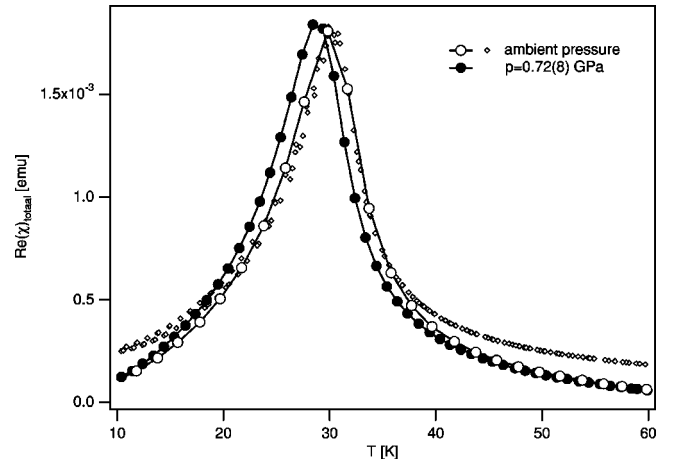


FIG. 7. Pressure dependence of the ac magnetic susceptibility in $\text{Er}_{0.6}\text{Pr}_{0.4}$ measured with $H_{dc}=0$ and $h_{ac}=10$ Oe at $f=1$ kHz [$\Delta T_C = -1.6(2)$ K/GPa, $\text{Re } \chi$ includes the background from the pressure cell and the calibrant, circles indicate measurements in pressure cell, and small diamonds without pressure cell (scaled)].

that the bump at $(T-T_0)/T_0 \sim -0.8$ (Fig. 6) results from the development of a basal component in the moment of Er and Pr, which has been already addressed in the preceding section (see, e.g., Fig. 4).

It was earlier conjectured that Er-Pr may show a magnetoelastic effect.⁶ Thus we have carried out measurements of the magnetization at elevated pressures on $\text{Er}_{0.6}\text{Pr}_{0.4}$. A pronounced dependence of the magnetic properties upon pressure may further lead to the presence of a barocaloric effect (BCE). The BCE is the pressure analogue to the MCE, i.e., a change of the $S_m(T)$ upon an applied external pressure which results in an extensive caloric effect ΔS or an intensive caloric effect ΔT , when applied isothermally or adiabatically, respectively.¹¹ The measured ac magnetic susceptibility of $\text{Er}_{0.6}\text{Pr}_{0.4}$ at ambient pressure and $p=0.7$ GPa are shown in Fig. 7. The ordering temperature T_0 is found to shift to lower temperatures by $dT_0/dp = -1.6(2)$ GPa/K. The sign and the size of dT_0/dp are in accordance with values found for the pure lanthanide metals and with theory. Specifically, in the RKKY model and the crude approximations of free electrons and isotropic elasticity, one finds $|J| \sim E_F^{-1} \sim a^2$, where E_F is the Fermi energy and a is the lattice parameter ($c \sim a \sim V^{1/3}$). Thus dT_0/dp is related to the bulk modulus B of the system

$$B = -\frac{2}{3} \left[\frac{1}{T_0} \frac{dT_0}{dp} \right]^{-1}. \quad (11)$$

With the above dT_0/dp for $\text{Er}_{0.6}\text{Pr}_{0.4}$ one finds $B = 13(2)$ GPa, which is within the same order of magnitude as the bulk modulus of the pure lanthanide metals ($B|_{\text{Er}} = 44$ GPa, $B|_{\text{Pr}} = 29$ GPa). With the moderate value of dT_0/dp , we infer the magnetoelastic effects to play a minor

role in $\text{Er}_{0.6}\text{Pr}_{0.4}$ and expect just a very small BCE for this alloy.

VI. CONCLUSIONS

The crystal field in the paramagnetic as well as in the Zeeman split case has been established for $\text{Er}_x\text{Pr}_{1-x}$ ($x = 0.6, 0.8$) by means of inelastic neutron scattering. The derived microscopic parameters were able to describe the specific magnetothermal properties of $\text{Er}_x\text{Pr}_{1-x}$ for $x \sim 0.7$, which have been determined by macroscopic measurements. Specifically, the ferrimagnetic alignment of the Er and Pr moments, their respective sizes, the observed MCE, and the enhancement of the magnetic entropy due to the addition of Pr can be reasonably well explained on the basis of a simple one-lattice mean-field approach coupling the two kinds of lanthanide ions. Therefore the modeling of a lanthanide based MCE material can be demonstrated by considering a set of just a few microscopic parameters. The CF in $\text{Er}_x\text{Pr}_{1-x}$ results in a pronounced anisotropy of the magnetic properties. Thus it is conjectured that a large MCE should be obtained on a single-crystal sample with the magnetic field ap-

plied along the c axis. No evidence has been found for a pronounced sensitivity of the magnetic ordering temperature on pressure in $\text{Er}_x\text{Pr}_{1-x}$ for $x \sim 0.6$.

ACKNOWLEDGMENTS

This work was performed at the Swiss Spallation Neutron Source SINQ, Paul Scherrer Institut (PSI), Villigen, Switzerland. We are indebted to Peter Allenspach (PSI), Thomas Mühlebach (PSI) and Rudolf Thut (PSI), for the help with the magnetic measurements under pressure. Financial support from the Swiss National Science Foundation (Grant No. 81EZ-68588) and the INFN, Sezione D: Magnetismo, Metalli, Superconduttività, Intervento Speciale, is gratefully acknowledged. The Ames Laboratory (AL) is operated by Iowa State University for the U.S. Department of Energy (DOE) under Contract No. W-7405-ENG-82. This research was supported by the Office of Basic Energy Sciences, Materials Sciences Division of the U.S. DOE (K.A.G., A.O.P., and V.K.P.). The authors wish to acknowledge Carl Schindler (AL) and David Kesse (AL) for their assistance in preparing the $\text{Er}_x\text{Pr}_{1-x}$ samples, and Ana Lima (AL) for her comments.

*Present address: Physique des Milieux Condensés, Université Pierre et Marie Curie B77 4 Place Jussieu, 75252 Paris, France. Email address: thierry.strassle@pmc.jussieu.fr

¹K. A. Gschneidner, Jr., V.K. Pecharsky, and M. Gailloux, in *Cryocoolers 8*, edited by R.G. Ross, Jr. (Plenum Press, New York, 1995), p. 685.

²K.A. Gschneidner, Jr., A.O. Pecharsky, and V.K. Pecharsky, *Cryocoolers 12*, edited by R.G. Ross, Jr. (Kluwer, Academic/Plenum Publishers, New York, 2003), p. 465.

³V.K. Pecharsky and K.A. Gschneidner, Jr., *J. Magn. Magn. Mater.* **200**, 44 (1999).

⁴K.A. Gschneidner, Jr. and V.K. Pecharsky, in *Intermetallic compounds*, edited by J.H. Westbrook and R.L. Fleischer, Principles and Practice, Vol. 3 (Wiley, New York, 2002), p. 519.

⁵Y.L. Wu, A.O. Pecharsky, V.K. Pecharsky, and K.A. Gschneidner, Jr., *Adv. Cryog. Eng.* **48**, 3 (2002).

⁶O. Moze, W. Kockelmann, Y.L. Wu, A.O. Pecharsky, V.K. Pecharsky, and K.A. Gschneidner, Jr., *J. Appl. Phys.* **91**, 8531 (2002).

⁷O. Moze *et al.* (unpublished).

⁸B. Bireckoven and J. Wittig, *J. Phys. E* **21**, 841 (1988).

⁹O. Moze, in *Handbook of Magnetic Materials*, edited by K. H. J. Buschow (Elsevier, Amsterdam, 1998), Vol. 11.

¹⁰B. Lebech, K.A. McEwen, and P.A. Lindgard, *J. Phys. C* **8**, 1684 (1975).

¹¹Th. Strässle, A. Furrer, Z. Hossain, and Ch. Geibel, *Phys. Rev. B* **67**, 054407 (2003).

¹²P. Touborg, *Phys. Rev. B* **16**, 1201 (1977).

¹³P. Touborg, R. Nevald, and T. Johansson, *Phys. Rev. B* **17**, 4454 (1978).

¹⁴J. Jensen and A. R. Mackintosh, *Rare Earth Magnetism* (Clarendon Press, Oxford, 1991).